Journal of Power Sources 195 (2010) 3186–3200

Contents lists available at ScienceDirect

Journal of Power Sources

journal homepage: www.elsevier.com/locate/jpowsour

Computational model to predict thermal dynamics of planar solid oxide fuel cell stack during start-up process

Jeongpill Ki, Daejong Kim*

Mechanical and Aerospace Engineering, The University of Texas at Arlington, 500 W. 1st Street, Arlington, TX 76019, United States

ARTICLE INFO

Article history:
Received 16 September 2009
Received in revised form
12 November 2009
Accepted 25 November 2009
Available online 2 December 2009

Keywords:
SOFC
Transient performance
Start-up
Thermal dynamics

ABSTRACT

Solid oxide fuel cell (SOFC) systems have been recognized as the most advanced power generation system with the highest thermal efficiency with a compatibility with wide variety of hydrocarbon fuels, synthetic gas from coal, hydrogen, etc. However, SOFC requires high temperature operation to achieve high ion conductivity of ceramic electrolyte, and thus SOFC should be heated up first before fuel is supplied into the stack. This paper presents computational model for thermal dynamics of planar SOFC stack during start-up process. SOFC stack should be heated up as quickly as possible from ambient temperature to above 700 °C, while minimizing net energy consumption and thermal gradient during the heat up process. Both cathode and anode channels divided by current-collecting ribs were modeled as one-dimensional flow channels with multiple control volumes and all the solid structures were discretized into finite volumes. Two methods for stack-heating were investigated; one is with hot air through cathode channels and the other with electric heating inside a furnace. For the simulation of stack-heating with hot air, transient continuity, flow momentum, and energy equation were applied for discretized control volumes along the flow channels, and energy equations were applied to all the solid structures with appropriate heat transfer model with surrounding solid structures and/or gas channels. All transient governing equations were solved using a time-marching technique to simulate temporal evolution of temperatures of membrane-electrode-assembly (MEA), ribs, interconnects, flow channels, and solid housing structure located inside the insulating chamber. For electrical heating, uniform heat flux was applied to the stack surface with appropriate numerical control algorithm to maintain the surface temperature to certain prescribed value. The developed computational model provides very effective simulation tool to optimize stack-heating process minimizing net heating energy and thermal gradient within the stack.

1. Introduction

Solid oxide fuel cell (SOFC) systems have been recognized as the most advanced power generation system with the highest thermal efficiency with a compatibility with wide variety of hydrocarbon fuels, synthetic gas from coal, hydrogen, etc. Department of Energy (DOE) Solid State Energy Conversion Alliance (SECA) program was initiated in 1999 [1] to develop utility scale SOFC-Gas turbine (GT) hybrid systems. Many companies [2–7] have been developing 3–10 kW SOFC systems under the SECA program as an intermediate step toward utility scale SOFC-GT hybrid. These small SOFC systems have their own novel markets such as distributed stationary power, residential homes, auxiliary power unit (APU) for heavy-duty trucks, and military applications.

Unlike other fuel cells, the operating temperature of SOFC is 800–1000 °C and the stack should be pre-heated to the operating temperature by electrical heating or by providing hot air through cathode channels. In laboratory level tests for material development or cell performance evaluations, the stack may be heated inside a furnace without constraint of energy usage for the heating. However, for SOFC-based power generation system to be stand-alone operating without too much involvement of operator, all the balance of plants (BOP) should be optimized for minimum energy consumption during start up.

Typical start-up procedure of the small SOFC-based system could be as follows; at first, fuel is supplied to combustor and air is supplied to combustor through heat exchanger and stack to generate thermal energy for heating of air and stack. External steam generator (or through steam separation unit from combustion gas) provides steam to the reformer and additional fuel is supplied to reformer. Once fuel cell begins to generate power, a steam management system (blower or ejector) may recirculate anode exhaust to reformer to provide high quality steam for continuous reforming of the fuel. Even at steady state, the combustor is essential to burn non-reacted residual fuel from the anode exhaust. Additional fuel supply to combustor is optional depending on operating conditions,

* Corresponding author. Tel.: +1 817 272 7620; fax: +1 817 272 5010.
E-mail address: daejongkim@uta.edu (D. Kim).

0378-7753/$ – see front matter © 2009 Elsevier B.V. All rights reserved.
doi:10.1016/j.jpowsour.2009.11.129

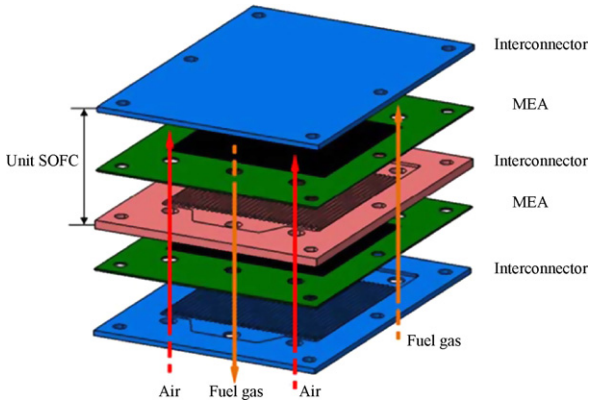

Fig. 1. Configuration of a planar SOFC.

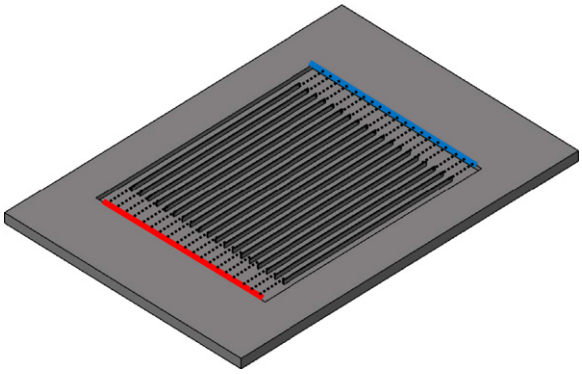

Fig. 2. Simplified interconnector model without assembly holes and inlet and exit holes replaced by straight inlet and exit regions.

such as heat exchanger inlet temperature control. As one can imagine, start up process of stand-alone SOFC system requires careful control of all the BOPs to minimize total energy consumption and minimize thermal stress in the stack. In transient operation following load demand or during start up, heat exchanger and stack may have the slowest thermal dynamics [8].

Design of "*stand-alone*" SOFC systems is quite challenging in terms of optimization of all BOPs and control strategy to minimize net energy consumption during start up. Even during normal operating modes, optimal control of fuel and air supply and anode gas recirculation relies on accurate dynamic model of the whole SOFC system.

Currently, most research activities were limited to component level characterization of single fuel cell stack in laboratory conditions or material research for catalyst and electrolyte, and thus design tools for "*SOFC system*" are quite lacking. Simulation works

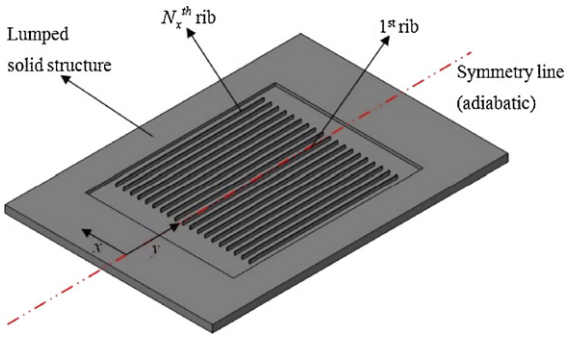

Fig. 3. Schematic of a discretized interconnector.

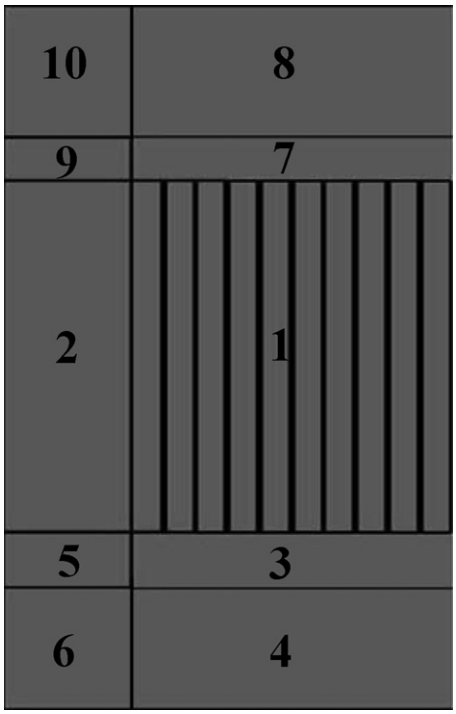

Fig. 4. Fractionized control volume.

may have different levels as follows:

Level 1: Steady state simulation of individual stack.
Level 2: Dynamic simulation of individual stack.
Level 3: Steady state simulation of SOFC system with external reformer, blowers, steam supply system, ducts, heat exchangers, etc.
Level 4: Dynamic simulation of SOFC system with external reformer, blowers, steam supply system, ducts, heat exchangers, etc.
Level 5: Steady state performance simulation of SOFC-GT hybrid systems with *lumped models* of SOFC and GT.
Level 6: Dynamic performance simulation of SOFC-GT hybrid systems with *realistic physical models* of SOFC and GT.

In the stack level, current simulation works are Level 1 with/out considering dynamics of stack temperature [9–11]. Achenbach [9] considers dynamics of stack temperature (partially Level 2) but continuity equations, other energy equations for gas species, and electrochemical reactions assume quasi steady state. Li et al. [11] simulated dynamic behavior of single planar SOFC stack by adopting time-dependent energy equations (partially Level 2) applied to both stack and gas flows. However, molar mass continuity equa-

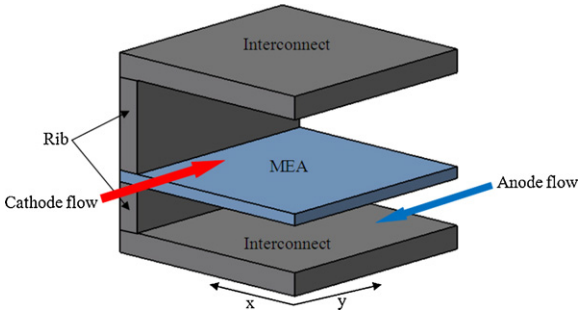

Fig. 5. (i, j)th unit element ($i = 1–N_x$, $j = 1–N_y$).

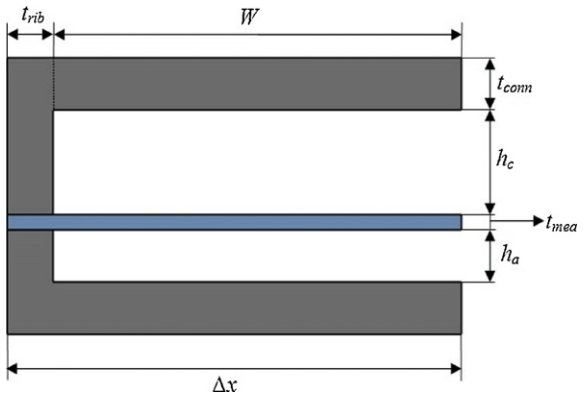

Fig. 6. Dimensions of an element of planar SOFC.

tions were at steady state and momentum equation and pressure drop along the flow directions were not considered.

Simulation works in Levels 3 and 4, which are important for design of stand-alone SOFC system are just few. Apfel et al. [12] considers the thermal start-up process of 5 kW planar SOFC stack for cathode and anode co-flow configuration. However, the thermal analyses on only discretized cathode and anode gas volumes were considered and detailed geometrical parameters of the stack are not provided. Rancruel and Spakovsky [13] simulate the start-up behavior of a SOFC-based auxiliary power unit including steam generator, reformer, and heat exchangers. Because all the subsystems and BOPs are considered in the simulation, accuracy of each subsystem is questionable. For example, heat exchangers which are similar to stack in terms of structure are modeled as lumped matrix and without considering thermal mass of gases. Ferrari et al. [14] presents early stage start-up behavior (before fuel cell electrochemical reaction begins) of a test rig mimicking SOFC-GT hybrid system consisted of emulators of turbomachinery, combustor, and stacks, and cathode recirculation ejector. The experimental verification of their Simulink®-based model was made for several start-up configurations. Barzi et al. [15] present transient model of tubular SOFC. The model includes detailed electrical circuit network through tubular SOFC anode and cathode layers, and transient continuity, momentum, and energy equations for gas channels and solid structures. Their transient model simulations use a simple time integration method with internal iterations to match local current densities and cell operating conditions.

These studies mentioned above emphasize importance of technical challenges involved in start-up behavior and transient operations of SOFC-based power generation systems. However, unfortunately none of these studies provide detailed geometry or

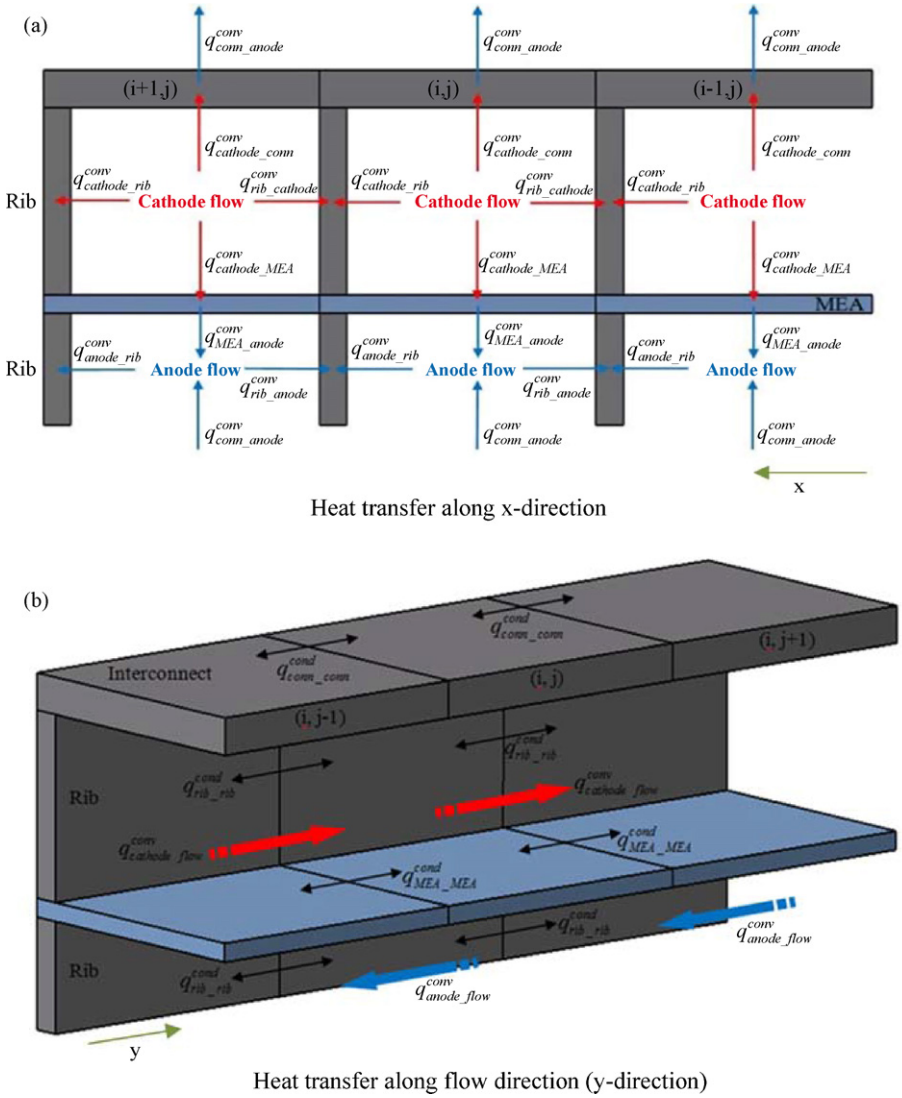

Fig. 7. Schematic diagrams of heat transfers in the SOFC stack: (a) Heat transfer along x-direction; (b) Heat transfer along flow direction (*y*-direction).

Table 1
Design of 1 kW SOFC stack.

Item	Unit	Value
Voltage	V	0.7
Current density	A cm^{-2}	0.51
Active cell area	cm^2	400
Number of stack	ea.	7
Anode flow	g s^{-1}	0.25457
Cathode flow	g s^{-1}	3.02253
Anode inlet composition (950 °C)		
H_2	%	50.66
H_2O	%	31.28
CO	%	16.67
CO_2	%	1.39

Table 2
Geometric dimensions of SOFC stack.

Element	Description	Size (mm)
W	Channel width	8
t_{rib}	Rib thickness	2
t_{conn}	Interconnect thickness	1
h_c	Cathode channel height	2
t_{mea}	MEA thickness	0.28 [25]
h_a	Anode channel height	1

Table 3
Properties of MEA [26–29].

Element	Property	Value
Membrane (YSZ)	Density (kg m^{-3})	5710
	Specific heat (J kg^{-1} K^{-1})	606
	Thermal conductivity (W m^{-1} K^{-1})	2.7
Anode (Ni-YSZ)	Density (kg m^{-3})	4460
	Specific heat (J kg^{-1} K^{-1})	595
	Thermal conductivity (W m^{-1} K^{-1})	6
Cathode (LSM)	Density (kg m^{-3})	4930
	Specific heat (J kg^{-1} K^{-1})	573
	Thermal conductivity (W m^{-1} K^{-1})	3

configuration of SOFC stacks that can be bench marked with any computational tool.

Simulations in Level 5 have been popular due to simplicity of lumped model of SOFC and GT [16–19]. In those works, SOFC is modeled as one control volume with single temperature and pressure with certain constraints of thermodynamic properties and inlet conditions.

Shelton et al. [20] present transient model for NETL Hybrid Performance Test facility using Simulink®. The model focuses on 1D model of duct flows and plenum dynamics. However, heat exchanger model is rather over-simplified without solving detailed energy, momentum, and mass continuity equations. Furthermore, SOFC module is missing because the model simulates GT power plant with dummy air plenum (to mimic SOFC) and ducts. Recently,

Table 4
Number of elements in each sub-domain in Fig. 4.

Region	x-Direction	y-Direction
1	10 (ribs number)	20
2	4	20
3	10	4
4	10	6
5	4	4
6	4	6
7	10	4
8	10	6
9	4	4
10	4	6

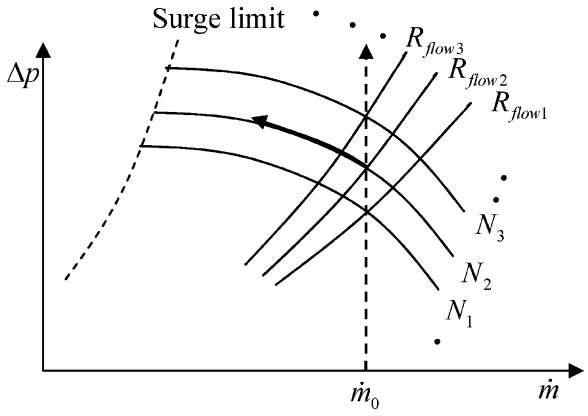

Fig. 8. Typical blower map under constant mass flow mode.

Mueller et al. [21] presents transient dynamic model of SOFC-GT hybrid including molar dynamic balance of species assuming system is at adiabatic. However, both anode and cathode channels are modeled as single control volumes.

The purpose of this paper is to develop thermal dynamic model of planar SOFC stack during start-up process using hot air through the cathode channels or electric furnace before fuel cell electrochemical reaction occurs. This work is a preliminary step toward Level 4 simulation described earlier. The ultimate goal of proper stack heating would be to minimize thermally induced stress within the stack and total energy consumption during the heating process. For the heating method using hot cathode air, mass flow rate and required pressure drop across the stack are closely coupled each other through channel geometry and temperature of the air inside the channel.

2. SOFC design and simulation work

Fig. 1 illustrates a planar SOFC stack consisting of the cathode, anode, electrolyte, and interconnector. In addition, Fig. 1 shows the fuel gas and air feed holes through the stack. Air exhaust hole is located on the other side of interconnector and fuel gas supply holes are also arranged similar way to air supply holes. Planar design is attractive since it is easy to manufacture and it uses less materials, hence potentially lower cost and high power density.

In real planar SOFC design, there are several connecting holes to join the structures. The locations and sizes of these holes are design-specific and there is no general rule for their sizes and locations. Therefore, for the modeling purpose, actual stack with these holes can be easily replaced by simpler stack model without these holes but with the same thermal mass as original one. There are also fuel gas and air feed holes through the stack as shown in Fig. 1.

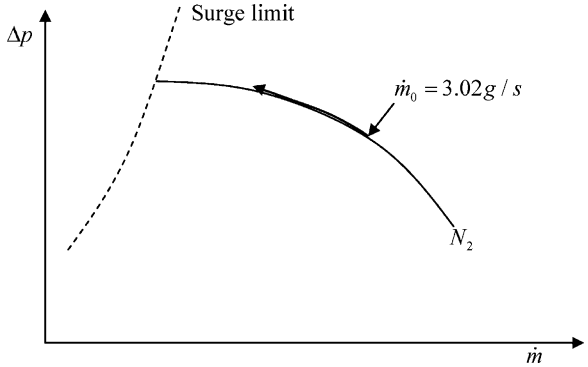

Fig. 9. Typical blower map under constant speed mode.

Inlet supply holes for fuel gas and air can be modeled as single thermodynamic condition as combination of inlet temperature and pressure. Therefore, the inlet and exit holes for fuel gas and air can be modeled as boundary conditions with certain pressures. In addition, the inlet holes are thermal boundary conditions as well as pressure boundary conditions. Considering these aspects, actual SOFC interconnect plate can be modeled as simple rectangular interconnect without these holes as shown in Fig. 2, where inlet and exit thermodynamic boundary conditions are applied to the boundaries represented as red and blue lines in the figure. The flow from the air and fuel gas inlet hole to the entrance of actual flow channels (divided by current collecting ribs) is mostly two-dimensional flow with certain (very small) pressure drop. Because the design of this region between the inlet air/fuel supply holes (see Fig. 1) to the entrance of the channels is also design-specific (each SOFC manufacturer has their own design), computational flow dynamic (CFD) simulation is the only method to analyze the detailed flow field. However, from thermal dynamics point of view of the stack, the detailed flow modeling for these inlet areas through computation-extensive CFD is not necessary. To capture realistic pressure drop and thermal interaction of the flow field with solid structures without sacrificing accuracy of the model, the flow field between the inlet represented as red line in Fig. 2 and the entrance of the channels is modeled as one-dimensional flows through virtual channels divided by infinitely thin ribs (shown as dotted lines in Fig. 2), which do not contribute to flow resistances.

3. Stack discretization

The model was developed for a single cell assuming entire stack would be made of multiple identical cells. The thermal and pressure boundary conditions are imposed on the air and fuel flow holes. Assuming the pressure drop across the vertical holes (manifolds in Fig. 1) are negligible and flow speed in these holes also small, identical thermal and pressure boundary conditions can be applied to all the cells. Of course the top and bottom cell's interconnectors are slightly different from the bipolar plates in the middle but these end effects were not considered.

Stack flow passages are divided into N_y control volumes along the flow direction (y), and number of passages is $2N_x$ for both anode and cathode channels as shown in Fig. 3.

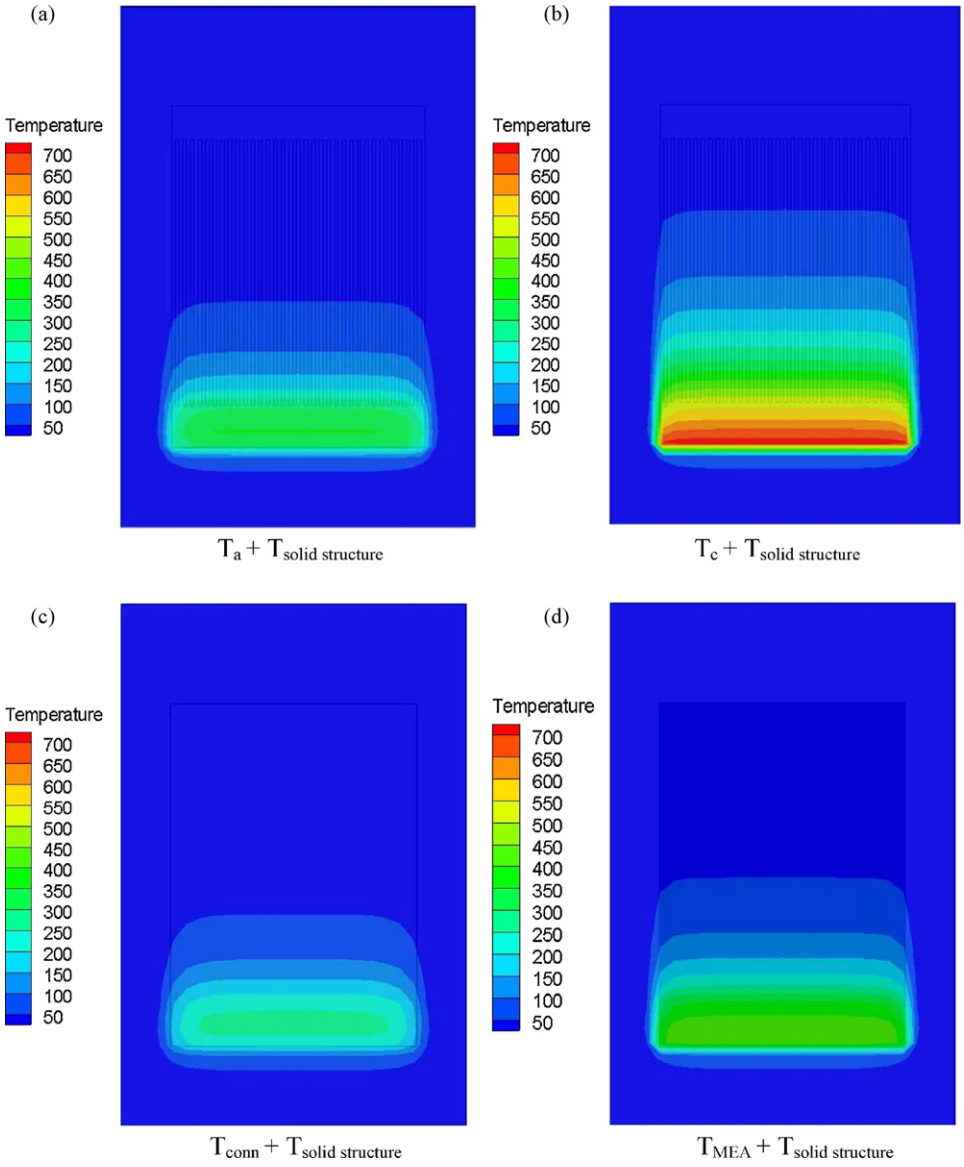

Fig. 10. Temperature distributions of gases and structures of SOFC stack (1 min): (a) $T_a + T_{solid\ structure}$; (b) $T_c + T_{solid\ structure}$; (c) $T_{Conn} + T_{solid\ structure}$; and (d) $T_{MEA} + T_{solid\ structure}$.

Becasuse of geometrical symmetry, simulations are performed for a half of the flow channels and stack centerline is treated as adiabatic. One side of interconnector plate may comprise total 10 sub-domains as shown in Fig. 4.

Domain 1 contains flow channels of air and fuel divided by ribs, domains 3 and 7 are flow entrance and exit regions without ribs and elctrochemical reactions, other domains are outer solid structures. The other side of interconnector plate is also divided by 10 sub-domains in a simiar way. All the domains with solid structures are also divided into multiple finite elements. Energy equation including storage terms is applied to each element to simulate temperature of each element in time domain.

Fig. 5 depicts (i, j)th unit element chosen from domain 1, with control volumes inside the element. Fig. 6 shows notations for dimensions used in the simulations. The analysis method presented in this paper can be simulated for both counter and parallel flow configurations. In this work, it is assumed the anode (fuel) and cathode (air) flows are in a counter flow configurations like Fig. 5. The inlet temperature and inlet pressures of the air and fuel gas (no fuel flow in this simulation) are specified as initial conditions.

4. Modeling

4.1. Momentum equation

If spatial fluctuation of mass flow rate inside the channel is not considered, i.e., $\partial\dot{m}/\partial x = 0$, mass flow rate is a function of only time. Using ideal gas law relating density, pressure and temperature, $\rho = P/R_{\text{gas}}T$, momentum equation for air flow along one-dimensional channel with hydraulic diameter of d_{h} is given by

$$\frac{\partial \dot{m}}{\partial t} = -A\frac{\partial p}{\partial x} - f_L \frac{\dot{m}^2}{2d_{\text{h}}} \frac{R_{\text{gas}}T_{\text{avg}}}{p_{\text{avg}}A} \tag{1}$$

where f_L is average Darcy friction factor [22] along the flow channel length, which are evaluated as

$$\begin{aligned} f_L &= \frac{1}{L}\int_0^L \frac{64}{Re_x}\,\mathrm{d}x: \quad \text{Laminar} \\ f_L &= \frac{1}{L}\int_0^L \frac{0.316}{\mathrm{Re}_x^{1/4}}\,\mathrm{d}x: \quad \text{Turbulent} \end{aligned} \tag{2}$$

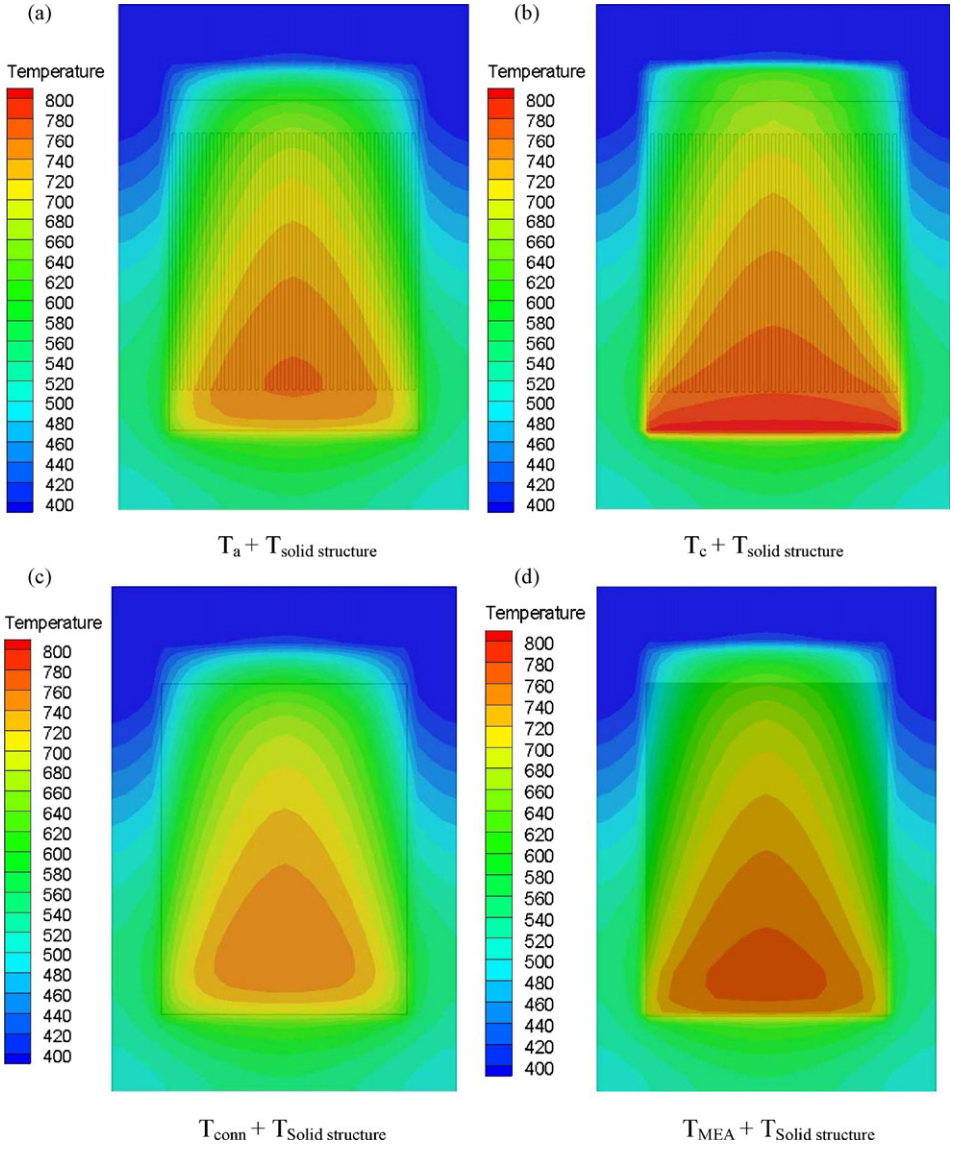

Fig. 11. Temperature distributions of gases and structures of SOFC stack (30 min): (a) $T_a + T_{\text{solid structure}}$; (b) $T_c + T_{\text{solid structure}}$; (c) $T_{\text{Conn}} + T_{\text{solid structure}}$; and (d) $T_{\text{MEA}} + T_{\text{solid structure}}$.

Because mass flux rate is a function of only time, $\partial p/\partial x$ should be constant throughout the channel

$$p = \Delta p\left(1 - \frac{x}{L}\right) + p_{\text{exit}} \tag{3}$$

where Δp is a pressure drop across the channel.

4.2. Energy equation to gas flow

If conduction within the gas and viscous heat dissipation are neglected, energy equation applied to both anode and cathode channels is written as

$$\frac{\partial T}{\partial t} = -\gamma\frac{RT}{p}\frac{\dot{m}}{A}\frac{\partial T}{\partial x} + \frac{RT}{p}\frac{\dot{q}_{\text{to\_gas}}}{c_{\text{v}}} \tag{4}$$

where $\gamma = c_{\text{p}}/c_{\text{v}}$. $\dot{q}_{\text{to\_gas}}$ is total heat flux input to the control volume of interest per unit volume, and it is given by

$$\dot{q}_{\text{to\_gas}} = \dot{q}_{\text{Conn\_gas}} + \dot{q}_{\text{MEA\_gas}} + \dot{q}_{\text{ribs\_gas}} \tag{5}$$

where $\dot{q}_{\text{Conn\_gas}}$ is convective heat transfer from interconnect to gas channel, $\dot{q}_{\text{MEA\_gas}}$ is convective heat transfer from MEA to gas channel, and $\dot{q}_{\text{ribs\_gas}}$ is convective heat transfer from ribs to gas channel. Heat convection coefficients are evaluated at corresponding reference film temperature which is an average temperature of gas in channel and surrounding solid structures. For example, reference film temperature for convection coefficient for cathode channel is an average temperature of cathode air channel, MEA, interconnect, and cathode ribs. Following Nusselt numbers [23] were used.

For laminar flow ($\text{Re} < 2300$)

$$Nu_{D_h} = 3.66 + \frac{0.0668\left(D_h/L\right)\cdot \text{Re}_{D_h}\cdot \text{Pr}}{1 + 0.04\left[\left(D_h/L\right)\cdot \text{Re}_{D_h}\cdot \text{Pr}\right]^{2/3}} \tag{6}$$

For turbulent flow ($\text{Re} \geq 2300$)

$$Nu_{D_h} = \frac{f/8\cdot(\text{Re}_{D_h} - 1000)\cdot Pr}{1 + 12.7\left(f/8\right)^{1/2}\cdot\left(Pr^{2/3} - 1\right)} \quad \text{where } f = \frac{0.316}{\text{Re}_{D_h}^{0.25}} \tag{7}$$

In most simulation conditions, flow was laminar. All the thermal properties such as Prandtl number and heat conduction coefficients were updated using temperatures found from previous time step in a frame of time integration scheme.

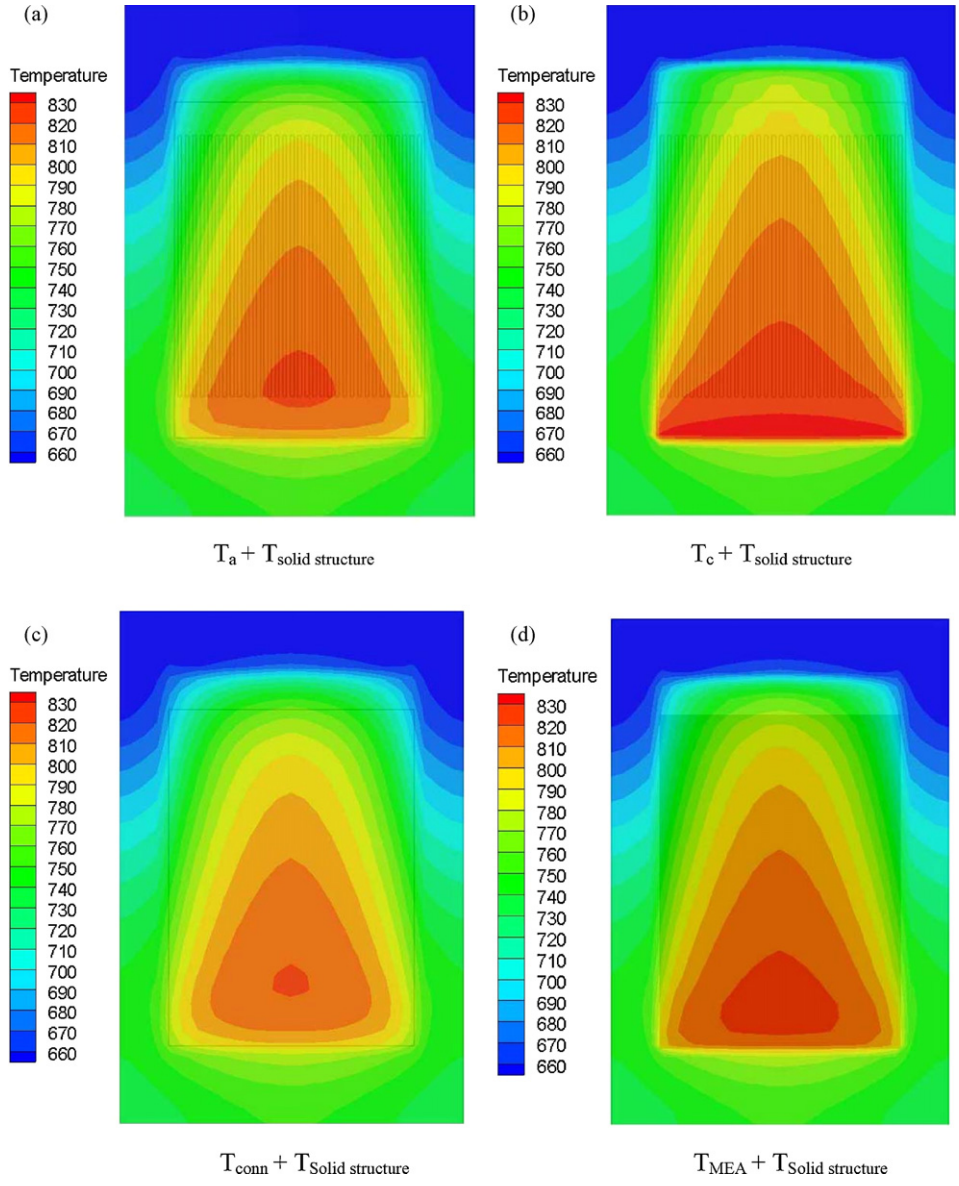

Fig. 12. Temperature distributions of gases and structures of SOFC stack (1 h): (a) $T_a + T_{\text{solid structure}}$; (b) $T_c + T_{\text{solid structure}}$; (c) $T_{\text{Conn}} + T_{\text{solid structure}}$; and (d) $T_{\text{MEA}} + T_{\text{solid structure}}$.

4.3. Energy equation to solid structures

Energy equation for MEA, interconnect, and ribs can be written as

$$\frac{\partial T_{\mathrm{MEA}}}{\partial t} = \alpha_{\mathrm{MEA}} \left(\frac{\partial^2 T_{\mathrm{MEA}}}{\partial x^2} + \frac{\partial^2 T_{\mathrm{MEA}}}{\partial y^2} \right) + \frac{\dot{q}_{\mathrm{to\_MEA}}}{\rho_{\mathrm{MEA}} c_{\mathrm{v\_MEA}}} \tag{8}$$

$$\frac{\partial T_{\mathrm{Conn}}}{\partial t} = \alpha_{\mathrm{Conn}} \left(\frac{\partial^2 T_{\mathrm{Conn}}}{\partial x^2} + \frac{\partial^2 T_{\mathrm{Conn}}}{\partial y^2} \right) + \frac{\dot{q}_{\mathrm{to\_Conn}}}{\rho_{\mathrm{Conn}} c_{\mathrm{v\_Conn}}} \tag{9}$$

$$\frac{\partial T_{\mathrm{Rib\_A/C}}}{\partial t} = \alpha_{\mathrm{Rib\_A/C}} \frac{\partial^2 T_{\mathrm{Rib\_A/C}}}{\partial x^2} + \frac{\dot{q}_{\mathrm{to\_Rib\_A/C}}}{\rho_{\mathrm{Rib\_A/C}} c_{\mathrm{v\_Rib\_A/C}}} \tag{10}$$

where α_{X} (X = MEA, Conn, Rib) are thermal diffusivities, and $\dot{q}_{\mathrm{to\_X}}$(X = MEA, Conn, Rib) are heat convection to corresponding structure from surrounding gas channels. The subscripts, A/C, denote anode and cathode respectively. Fig. 7 shows all the heat transport mechanisms (excluding radiation) within the stack including convections (superscript "conv") and conductions (superscript "cond") with their appropriate directions. Referring to Fig. 7 (a), heat flux terms in above equations are

$$\dot{q}_{\mathrm{to\_MEA}} = \dot{q}^{\mathrm{conv}} - \dot{q}^{\mathrm{conv}} \tag{11}$$

$$\dot{q}_{\mathrm{to\_Conn}} = \dot{q}^{\mathrm{conv}} - \dot{q}^{\mathrm{conv}} \tag{12}$$

$$\dot{q}_{\mathrm{to\_Rib\_}A} = \dot{q}^{\mathrm{conv}} \tag{13}$$

$$\dot{q}_{\mathrm{to\_Rib\_}C} = \dot{q}^{\mathrm{conv}} \tag{14}$$

Eqs. (1), (4) and (8)–(10) comprise complete set of non-linear differential equations for local gas temperature, local mass flow rate, and local temperature of MEA and interconnect. Boundary conditions are inlet gauge pressure, $p_{\mathrm{gauge\_inlet}}(t)$, with respect to exit pressure (i.e., pressure drop), and initial conditions for temperatures are all ambient temperature and initial conditions for mass flow rates in all the channels are zero.

In the simulation, hot air at constant temperature of 850 °C is provided to the cathode channels at the inlet (the boundary between regions 3 and 4). In regions 3 and 7 in Fig. 4, it is assumed that the flow is one dimensional through virtual flow channels divided by infinitely thin ribs, which do not contribute to flow resistances. Flow momentum and energy equations are applied

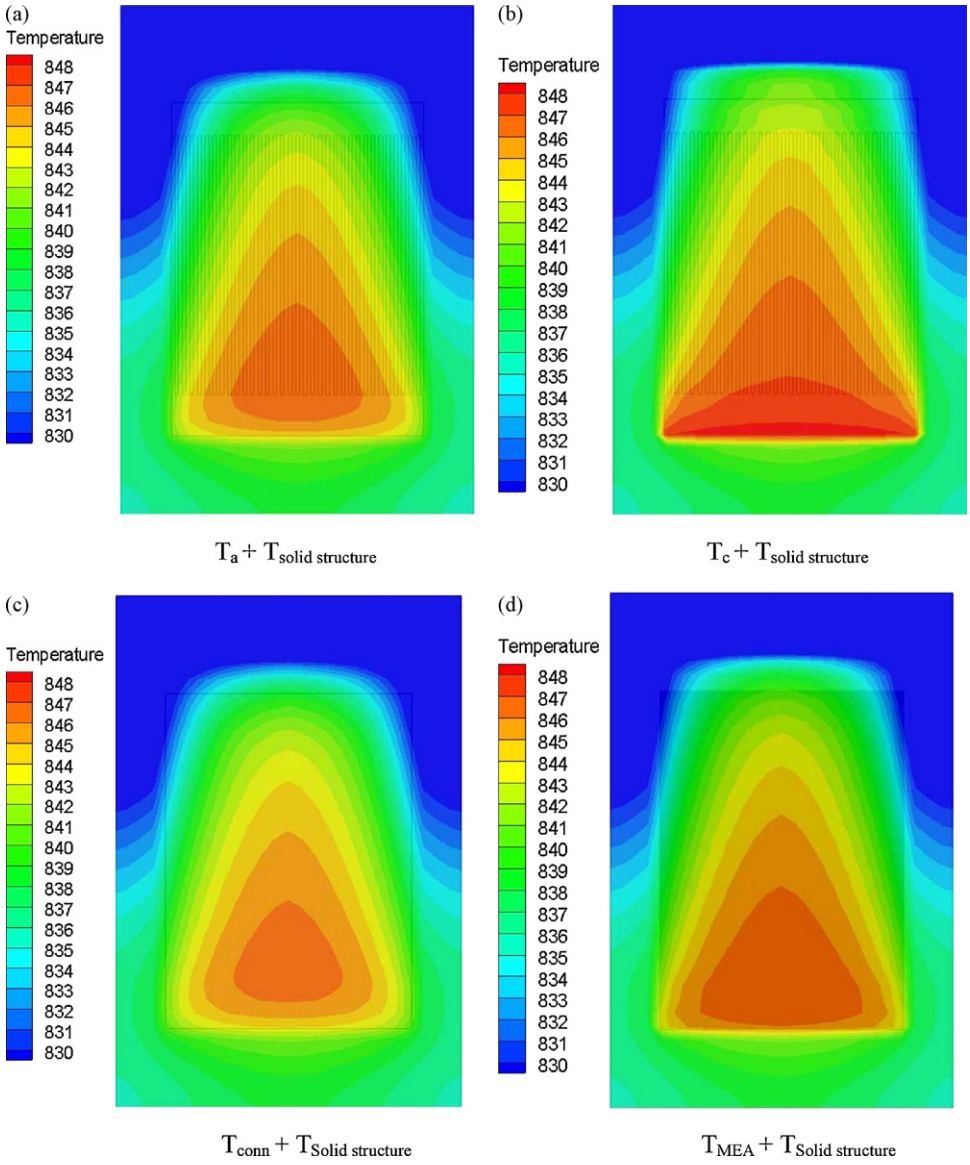

Fig. 13. Temperature distributions of gases and structures of SOFC stack (2 h): (a) $T_a + T_{solid\ structure}$; (b) $T_c + T_{solid\ structure}$; (c) $T_{Conn} + T_{solid\ structure}$; and (d) $T_{MEA} + T_{solid\ structure}$.

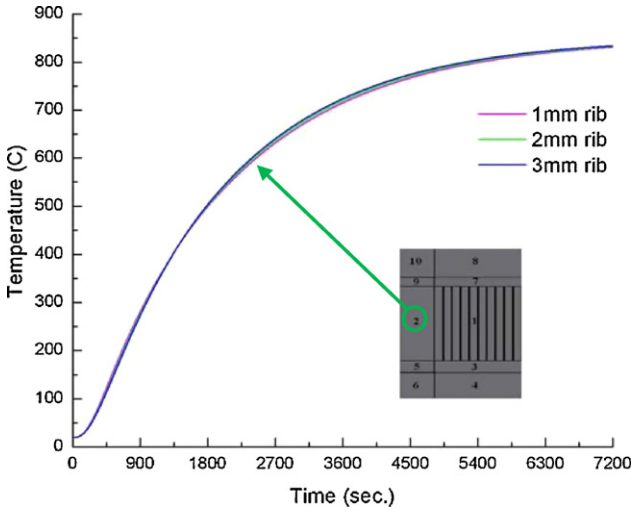

Fig. 14. Temperature on central area of 2nd solid structure in Fig. 4.

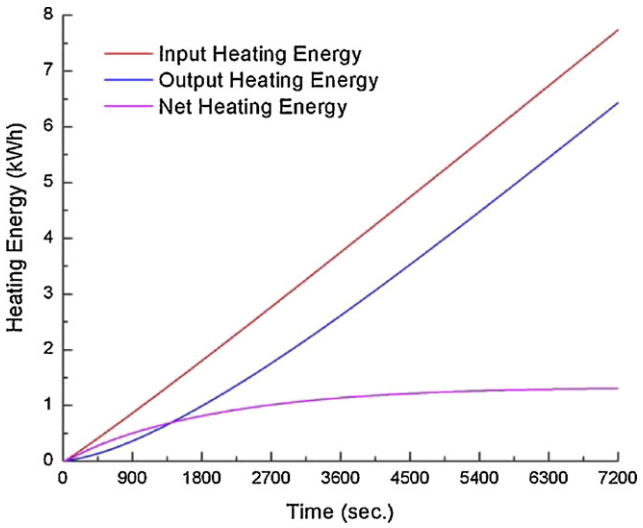

Fig. 16. Heating energy vs. time (hot air feeding method).

to these virtual flow channels in regions 3 and 7. Energy equations are applied to solid structures in these regions. Pressure drop is specified between inlet and exit of the stack and local pressures at the entrance and exit of the flow channel areas (boundary between regions 3 and 1 and boundary between regions 1 and 7) are internally calculated through mass conservation at these boundaries.

4.4. Discretization

All the first and second derivative terms in governing equations are discretized with the central difference method [24];

$$\left(\frac{\partial T}{\partial x}\right)_{i,j} = \frac{T_{i+1,j} - T_{i-1,j}}{2\Delta x}, \quad \left(\frac{\partial T}{\partial y}\right)_{i,j} = \frac{T_{i,j+1} - T_{i,j-1}}{2\Delta y} \tag{15}$$

$$\left(\frac{\partial^2 T}{\partial x^2}\right)_{i,j} = \frac{T_{i+1,j} - 2T_{i,j} + T_{i-1,j}}{\Delta x^2},$$

$$\left(\frac{\partial^2 T}{\partial y^2}\right)_{i,j} = \frac{T_{i,j+1} - 2T_{i,j} + T_{i,j-1}}{\Delta y^2} \tag{16}$$

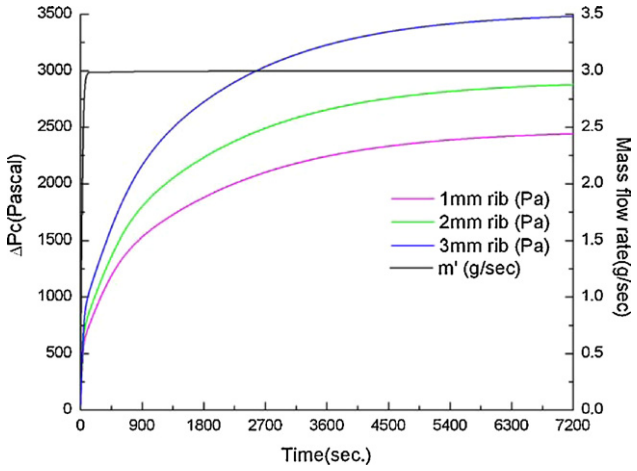

Fig. 15. Required pressure drop over time to maintain the required mass flow rate.

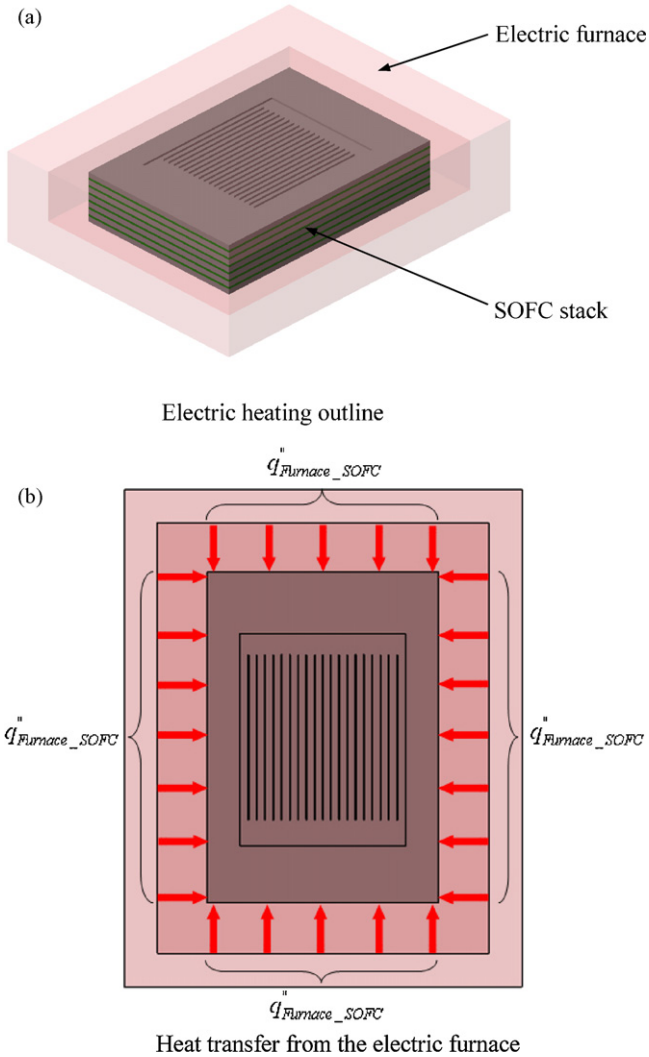

Fig. 17. Schematic diagrams of heat transfer from Furnace to the SOFC stack: (a) electric heating outline and (b) Heat transfer from the electric furnace.

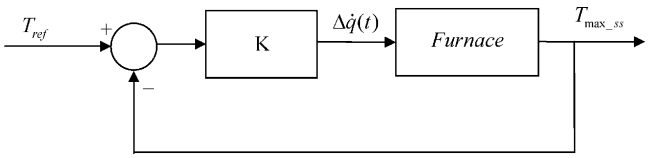

Fig. 18. Block diagram of simple proportional control for furnace heating.

5. Results

Typical heating methods of SOFC stack would be either electrical heating inside a furnace or using hot air through the cathode flow channels while the stack is insulated. The developed models in this paper were applied to stack-heating using both methods.

1 kW SOFC system was designed and simple thermodynamic analyses were performed to estimate typical cathode air flow rate needed for the 1 kW SOFC. Preliminary 1 kW SOFC stack flow channel dimensions were chosen based on steady state operating conditions assuming the fuel-gas stream is generated from methane (CH_4) auto thermal reformer (ATR) with the following balanced equations

$$CH_4 + 0.5\lambda(O_2 + 3.76N_2) + (1-\lambda)H_2O \leftrightarrow CO + (3-\lambda)H_2 + 1.88\lambda N_2 \quad (17)$$

$$CO + H_2O \leftrightarrow H_2 + CO_2 \quad (18)$$

where air-to-fuel ratio $\lambda \approx 0.2$–0.3 is typically used. Equilibrium composition of ATR exit was calculated using principle of minimization of Gibb's energy of formation assuming ATR exit temperature is at 950 °C at $\lambda = 0.3$. Table 1 summarizes design of 1 kW SOFC stack for oxygen utilization factor of 0.17 and fuel utilization factor of 0.8. Steam-to-carbon ratio is about 1.88. The cathode air flow rate, 3.02 g s^{-1}, calculated in Table 1 was used as cathode air flow rate for heating the stack.

In addition, the electrolyte-supported SOFC was chosen to be simulated because this type has better chemical tolerance at high temperature.

Table 2 provides physical dimensions of the designed SOFC stack, and Table 3 shows the thermo-mechanical properties of MEA. In this simulation, thermo-mechanical properties of MEA are

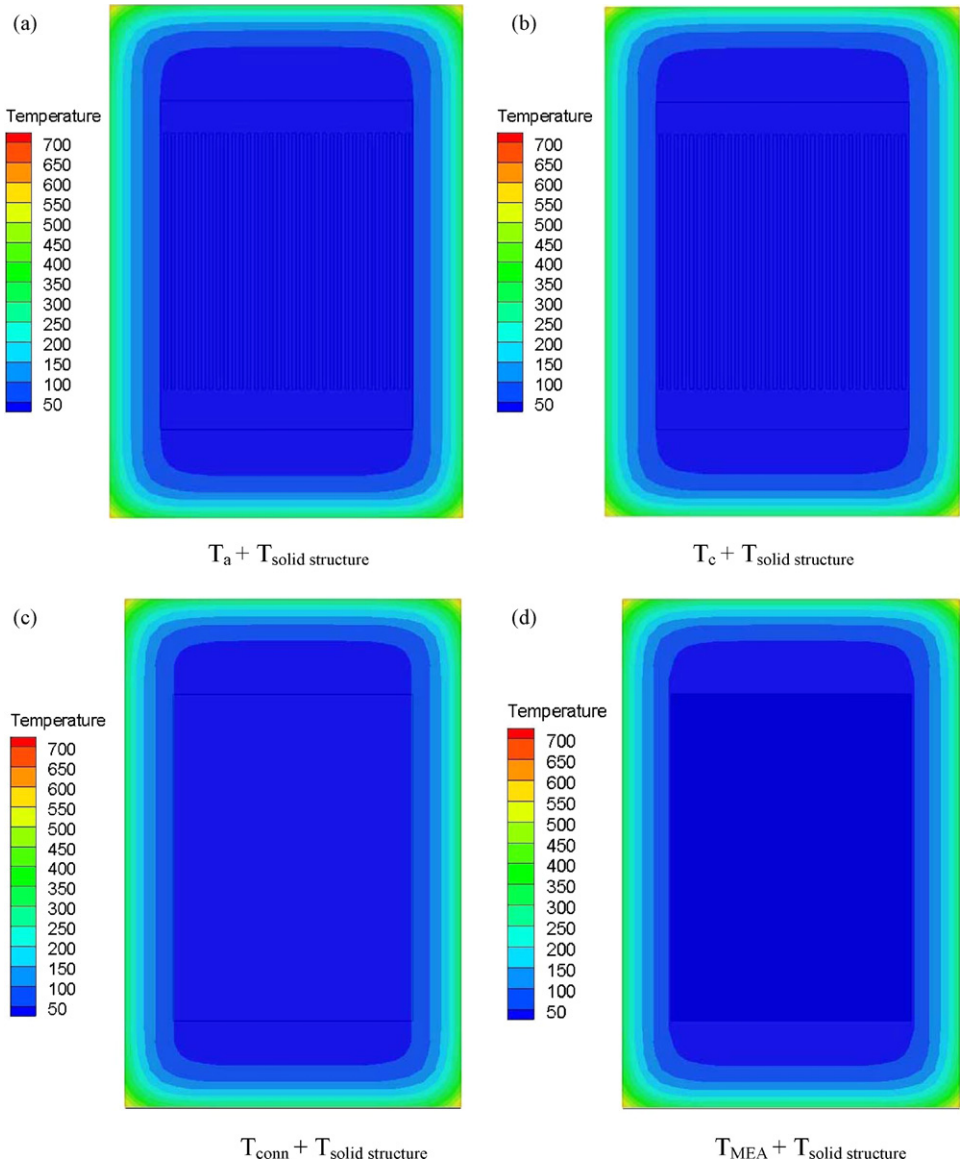

Fig. 19. Temperature distributions of gases and structures of SOFC stack (1 min): (a) $T_a + T_{solid\ structure}$; (b) $T_c + T_{solid\ structure}$; (c) $T_{Conn} + T_{solid\ structure}$; and (d) $T_{MEA} + T_{solid\ structure}$.

assumed to follow those of YSZ because the thickness of anode and cathode is relatively smaller than YSZ.

In this simulation, the cathode air at 850 °C was supplied at cathode inlet, while there is no feeding of anode gases at anode inlets. All the faces of solid structures exposed to surrounding are assumed to be adiabatic (insulated). Number of segmental elements in each domain shown in Fig. 4 is summarized in Table 4.

In the case of stack-heating using hot cathode air, two blower operating modes can be considered; one is constant mass flow mode and the other is constant speed mode. As stack is being heated up, flow resistance increases with temperature along the flow channel, and mass flow rate decreases gradually over time if the total pressure-drop across the stack is maintained constant. Therefore, if constant mass flow rate across the stack is desired during the heat up, the blower operating points should follow vertical dotted line shown in Fig. 8, i.e., the blower speed should be increased to follow the required inlet pressure.

Another operating mode is at constant blower speed. When the blower is operated at constant speed, both pressure and mass flow rate change while stack is heated up. Because the blower is operated

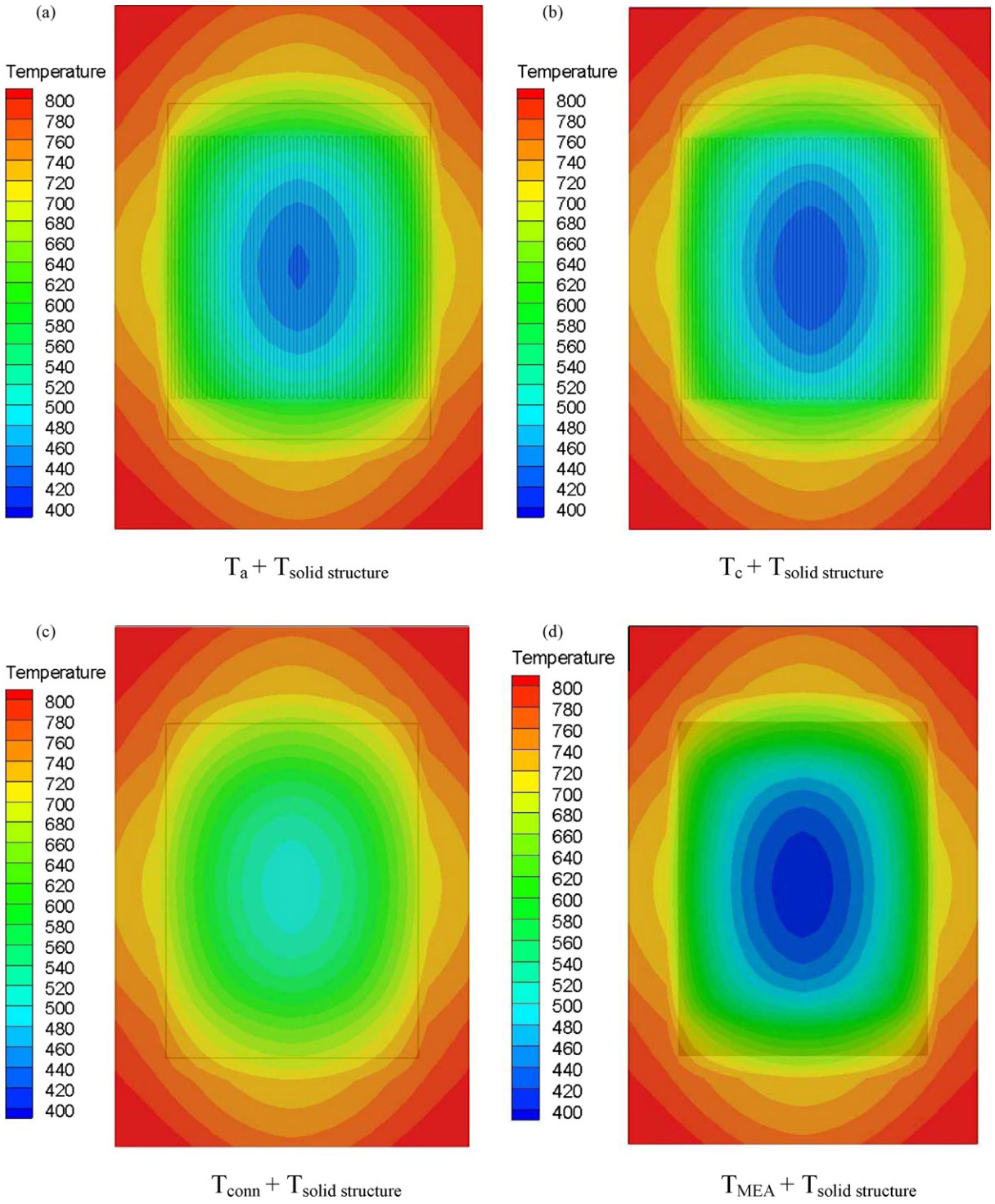

Fig. 20. Temperature distributions of gases and structures of SOFC stack (30 min): (a) $T_a + T_{solid\ structure}$; (b) $T_c + T_{solid\ structure}$; (c) $T_{Conn} + T_{solid\ structure}$; and (d) $T_{MEA} + T_{solid\ structure}$.

at constant speed, the operating point follows the constant speed curve in the blower performance map as shown in Fig. 9. Depending on the initial blower setting speed, blower can suffer surge before the stack reaches desired temperature if the flow resistance inside the stack increases beyond the blower surge limit.

Because blower performance map is not available, simulations were performed for only constant mass flow rate mode, and required pressure drop to maintain the specified air mass flow rate was calculated at each time step. Once blower map of appropriate blower is available, constant speed mode could be simulated.

Figs. 10–13 show the temperature distributions over solid structure, rib, MEA, interconnect, and each channel after 1 min, 30 min, 1 h, and 2 h, respectively. Figures (a) represent the temperature distributions of the anode gases and outer solid structures. Figures (b) show the temperature distributions of the cathode gases and solid structures. Figures (c) show the temperature distributions of interconnect and solid structures. Finally, the temperature distributions of MEA and outer solid structures are portrayed in Figures (d). In the early stage, the heat transfer occurs uniformly along *x*- and *y*-direction. As time goes by, the high temperature distribution concentrates in the middle area because there are bulk solid structures as large heat sink outside electrochemically active area. Also, the figures indicate that the maximum temperature zone is distributed widely throughout the cathode air inlet during the start-up. The downstream solid structures from the cathode inlet area have lower temperature all the time.

The difference of temperature between air inside the cathode and anode channels was caused by the different channel height (hc = 2 mm, ha = 1 mm in Table 2) and the larger thermal conductivity of interconnect compared to MEA. Therefore, it is reasonable that interconnect has relatively high temperature distribution compared to MEA. Fig. 14 represents the evolution of temperature at the center of the stack outer solid structure. As Fig. 14 shows, the temperature of solid structure increases rapidly from 20 °C to about 650 °C and then increases gradually to final steady state temperature. In addition, the small difference of rib thickness does not affect to the temperature of solid structures because the volume of total rib is much smaller than the total volume of solid structures.

As was mentioned before, simulation was performed with a constant air mass flow rate of 3.02 g s^{-1} (cathode air flow rate during normal operation from Table 1). A simple numerical control algorithm was implemented to adjust pressure drop internally at every time step to maintain the specified mass flow rate. Fig. 15 plots pressure drop across the stack to maintain the constant flow

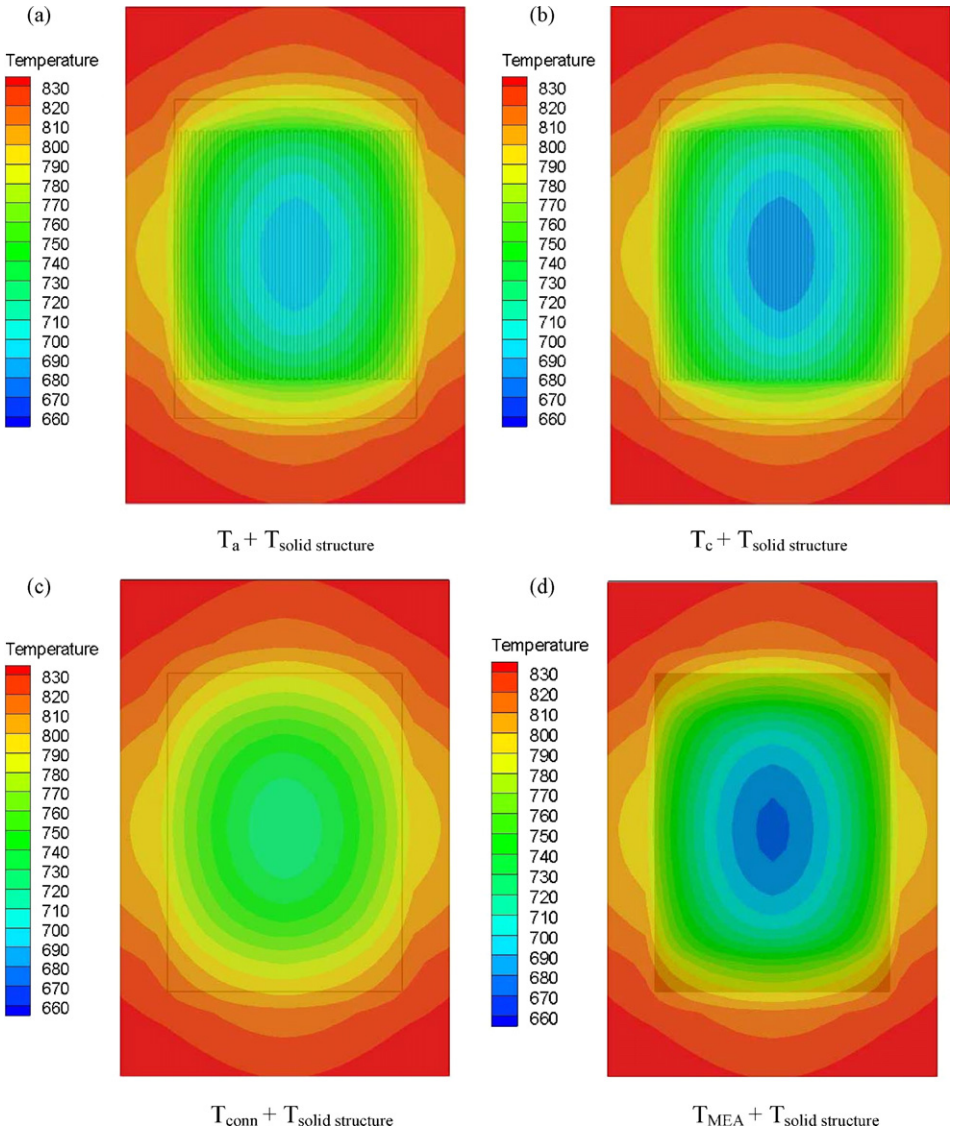

Fig. 21. Temperature distributions of gases and structures of SOFC stack (1 h): (a) $T_a + T_{solid\ structure}$; (b) $T_c + T_{solid\ structure}$; (c) $T_{Conn} + T_{solid\ structure}$; and (d) $T_{MEA} + T_{solid\ structure}$.

rate of 3.02 g s^{-1} with different rib sizes. Notably, for 2 mm rib, the required pressure drop increases from around 40 Pa to almost 2877 Pa after 2 h of heating. The bigger rib size shows the larger pressure drop. In addition, it takes about 6450 s (≅1.79 h) to reach the minimum temperature of 800 °C within the stack. During that time, net heating energy of 1.2926 kWh is required as shown in Fig. 16.

However, the heating method using the hot air feeding results in poor thermal efficiency. The heating efficiency was calculated by equation below and is at most around 17%.

$$\eta_e = \frac{\text{Net heating energy}}{\text{Input heating energy}} = \frac{1.30651}{7.73926} = 0.1688 \quad (19)$$

A large amount of heating energy is lost through the exit flow out of the stack without contributing to heating of SOFC stack, especially toward the end of heating once stack has reached certain high temperature. However, in actual SOFC systems with heat exchangers and combustor, this stack exit flow would be directed to combustor with reduced fuel flow rate to the combustor if constant combustor exit temperature is required for the gas heat exchanger at the downstream which is used to generate hot cathode air for stack heating. In addition residual heat energy would be used for steam generation or fuel heating, etc. Therefore, actual efficiency in terms of total energy consumption during the heating would be much higher than that from (19).

Another stack heating method using electric furnace was simulated with all the cathode and anode channel flows as zero. In this heating method, a SOFC stack is inside an electric furnace as Fig. 17(a). In this analysis, there is two-dimensional heat input shown as Fig. 17(b) through the outer solid structure domains (2, 4, 5, 6, 8, 9 and 10 of Fig. 4) from furnace to SOFC stack. In addition, the upper and lower sides are assumed to be insulated; this assuption is reasonable because bottom surface of the stack should sit on certain structure and the structure cannot be a heating element.

Preliminary simulation with fixed heat flux of 1000 W results in rapid and continuous increase of stack surface temperature above 1000 °C, while inside temperature remains below 200 °C because of large thermal mass of the stack and large heat transfer resistance through thin MEA and interconnect. To avoid high thermal gradient that causes thermal stress during heating process, heat flux should be controlled to keep the surface temperature within certain limit. The easiest and practically used method in actual electrical heating is to use simple control algorithm to adjust heating rate. Any change

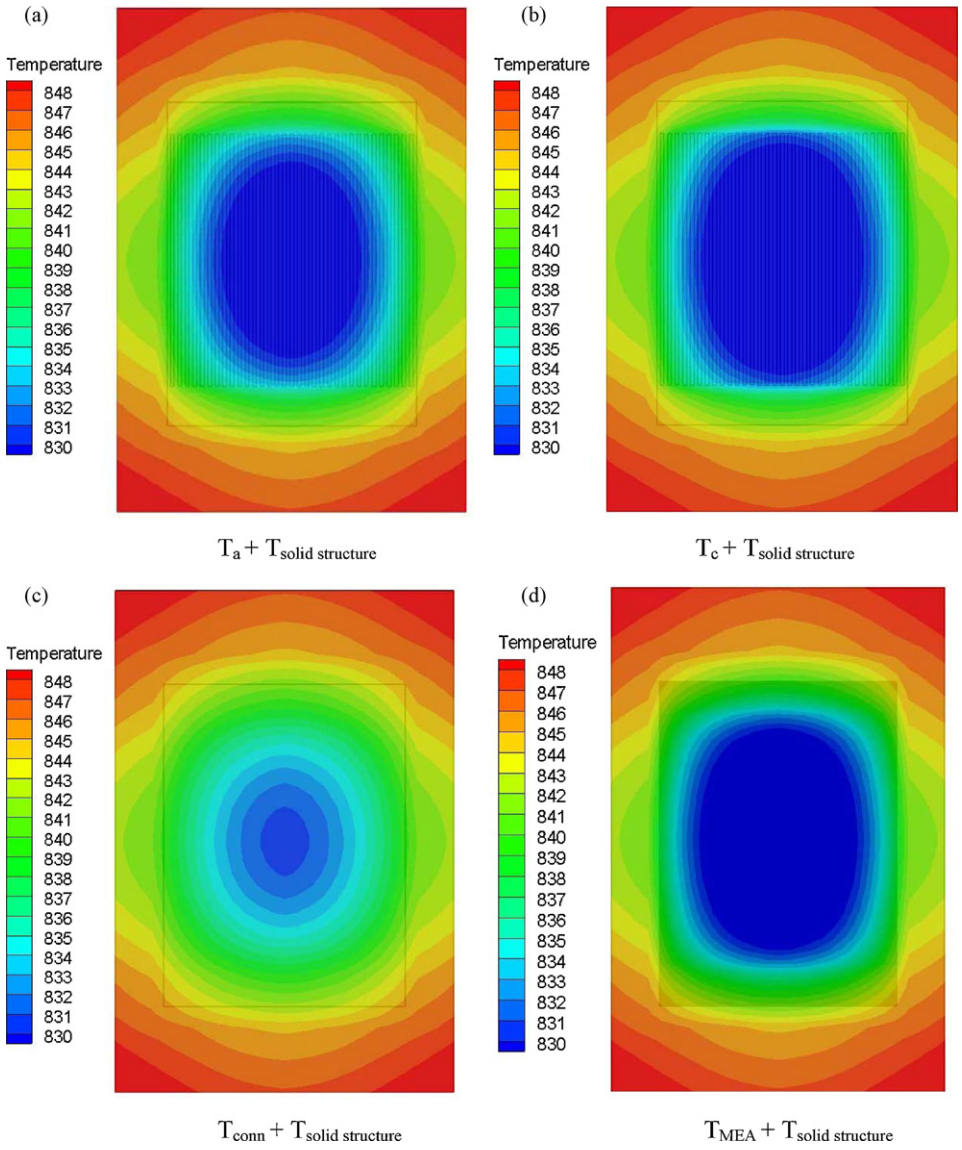

Fig. 22. Temperature distributions of gases and structures of SOFC stack (2 h): (a) $T_a + T_{solid\ structure}$; (b) $T_c + T_{solid\ structure}$; (c) $T_{Conn} + T_{solid\ structure}$; and (d) $T_{MEA} + T_{solid\ structure}$.

of heating rate at certain time would be

$$\Delta\dot{q}(t) = K(T_{\text{ref}} - T_{\text{max\_ss}}) \quad (20)$$

where K is proportional gain, $T_{\text{max\_ss}}$ is maximum surface temperature of soild structrue and T_{ref} is a reference temperature of 850 °C. Block diagram of the numerical control algorithm is shown in Fig. 18.

One specific numerical value of input heating energy can be set as an initial condition. Initial heating power was chosen as 1000 W with gain K=100. With K=100, overall SOFC stack temperature distribution can be found in Figs. 19–22. These figures depict the temperature distribution over solid structure, rib, MEA, interconnect, and each channel after 1 min, 30 min, 1 h and 2 h, respectively. As shown in the figures, all temperature distributions are symmetrical because chosen stack is geometrically symmetric and uniform heat flux is applied at all surfaces.

Unlike the heating method using cathode air, there is no distinctive difference of temperature distributions between structures and channels at the beginning. In addition, temperature gradient is always from outer surface to inside. The increase of temperature of anode channel is faster than cathode due to the shorter height of channel. In addition, the increase of temperature of interconnect is faster than MEA due to its larger thermal conductivity than MEA.

Because heating rate is adjusted following Eq. (20), once stack surface temperature reaches prescribed maximum allowable temperature, net heating energy can be found using the following equation

$$E_{\text{Furnace}} = \int_0^{t_{\text{end}}} \dot{q}(t)\ \mathrm{d}t \quad (21)$$

When initial heating rate of 1000 W was chosen, total heating energy until lowest temperature over entire stack reaches 800 °C was found as 1.8768 kWh using (21) for total heating time of 5980 s (≅1.66 h). Depending on initial heating rate, transient behavior of stack surface temperature can be different. Fig. 23 shows the net heating energy for 2 h for two different initial heating rates of 100 W and 1000 W. As Fig. 23 implies, initial heating rate of 1000 W causes rapid increase of stack surface temperature while initial heating rate of 100 W gradually increases the stack surface temperature allowing less thermal gradient in the stack.

Fig. 24 shows the net heating energy that was supplied to SOFC stack with the electric furnace for 2 h for different rib sizes. As shown in Fig. 24, the net heating energy was not affected much (only 2–3% difference of net heating energy) by changing the rib sizes from 1 mm to 3 mm because total rib volume is negligible compared to the total stack volume.

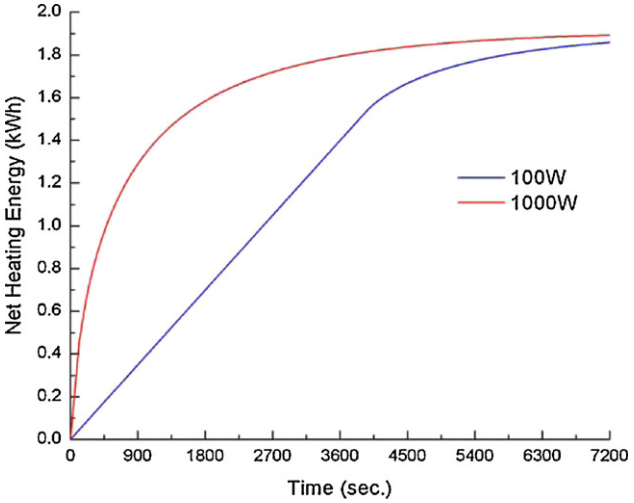

Fig. 23. Net heating energy with different furnace heat inputs.

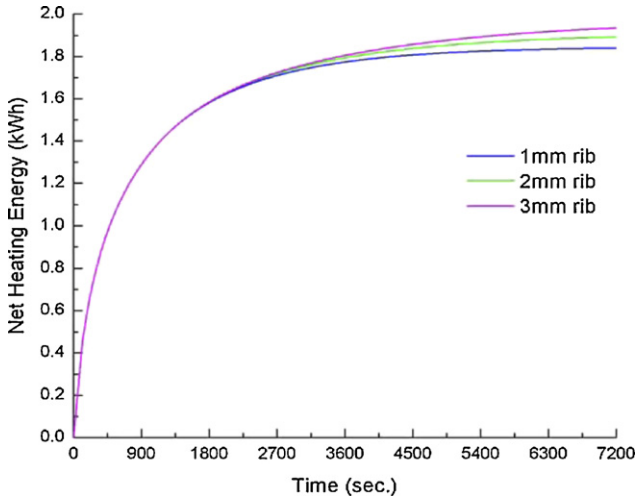

Fig. 24. Net heating energy vs. time (furnace heating).

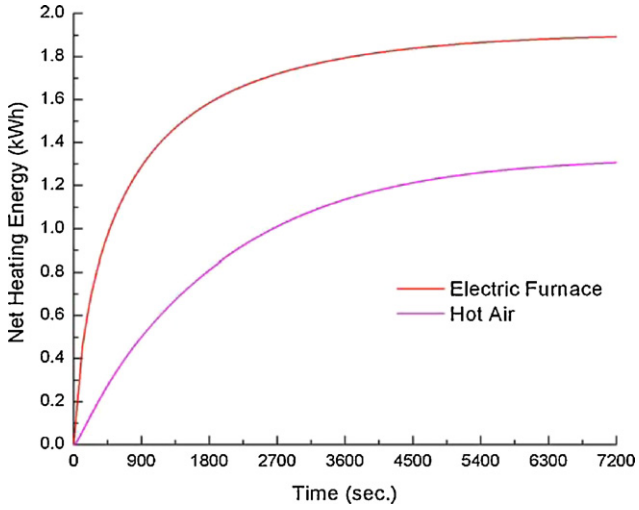

Fig. 25. Net heating energy comparison between furnace and hot air heating method.

Fig. 25 compares the net heating energy for both heating methods. When only net heating energy is considered, hot air heating method requires less net heating energy than electric furnace heating method. The temperature range of whole SOFC stack with hot air heating for 1 h is within around 202–220 °C, while around 128–172 °C with furnace heating for 1 h. In addition, after 2 h of heating, the temperature ranges are 29–31 °C for hot air heating and 19–27 °C for furnace heating. However, different initial heating rates for furnace heating result in different thermal gradient inside the stack. Likewise, different hot air flow rates result in different thermal gradient inside the stack. Therefore, heating rates or hot air flow rates should be controlled accordingly depending on allowable maximum thermal stress or thermal gradient for specific stack design.

6. Conclusions

Computational model was developed to find temperature distributions of solid structures and gas channels in a SOFC stack during start up process using both cathode hot air and electrical furnace heating. Using the developed model, temperature distribution of

solid structures and gas channels can be found at any specific time step. The computational model is a very effective tool to understand thermal transient response of stack during start-up heating.

The model was applied to 1 kW planar SOFC stack to investigate transient behavior of the stack during both hot cathode air heating and electrical heating inside the furnace. For the case of using hot cathode air with constant mass flow rate, inlet pressure required to maintain the constant mass flow rate increases significantly over time as the flow resistance inside stack increases with temperature. Selection of air blower and its required performance map should be tuned to meet the pressure requirement for proper air delivery.

Electrical heating requires controlled heating to avoid rapid temperature rise of the stack surface. Depending on thickness of MEA and interconnects, thermal conduction through these thin structures varies and heating rate should be controlled accordingly to avoid large thermal gradient during the heating.

Both heating methods require similar net heating energy to achieve uniform stack temperature within prescribed limit. However, air heating with constant mass flow rate results in waste of large amount of heat energy through exiting air with high enthalpy. Operating the blower at constant speed mode allows the gradual decrease of air mass flow rate when stack is heated and may result in higher heating efficiency. However, for either constant mass flow rate or constant speed case, thermal energy of the exiting air should be recovered through heat exchangers for reformer or steam generator which are integral parts of most SOFC systems.

References

[1] DOE SECA Program, Available at http://www.Netl.Doe.Gov/Technologies/Coalpower/Fuelcells/Seca/.
[2] SOFC Developer: Acumetrics Corporation, Available at http://www.Acumentrics.Com/Products-Power-Generators.Htm.
[3] SOFC Developer: Cummins Power Generation, Available at http://www.Cumminspower.Com/Na/About/Environmental/Fuelcells/.
[4] SOFC Developer: Delphi Automotive Systems LLC, Available at http://Delphi.Com/Manufacturers/Auto/Fuelcells/Seca/.
[5] SOFC Developer: Fuel Cell Energy, Inc., Available at http://www.Fuelcellenergy.Com/Files/Sofc%20thrust%20area.Pdf#Search="Seca".
[6] SOFC Developer: Siemens Power Generation, Available at http://www.Powergeneration.Siemens.De/Products-Solutions-Services/Products-Packages/Fuel-Cells/Seca-Program-Schedule/.
[7] Developer of SOFC-MGT Hybrid: Siemens Westinghouse, Available at http://www.Powergeneration.Siemens.Com/Products-Solutions-Services/Products-Packages/Fuel-Cells/Sofc-Gt-Hybrid/Sofc-Gt-Hybrid.Htm.
[8] A. Traverso, A.F. Massardo, R. Scarpellini, Applied Thermal Engineering 26 (16) (2006) 1935–1941.
[9] E. Achenbach, Journal of Power Sources 49 (1994) 333–348.
[10] P. Costamagna, K. Honegger, Journal of Electochemical Society 145 (11) (1998) 3995–4007.
[11] J. Li, G.Y. Cao, X.J. Zhu, H.Y. Tu, Journal of Power Sources 171 (2007) 585–600.
[12] H. Apfel, M. Rzepka, H. Tua, U. Stimming, Journal of Power Sources 154 (2006) 370–378.
[13] D. Rancruel, M. Spakovsky, International Journal of Thermodynamics 8 (2005) 103–113.
[14] M. Ferrari, A. Traverso, M. Pascenti, A. Massardo, Journal of Power and Energy 221 (2007) 627–635.
[15] Y. Barzi, M. Ghassemi, M. Hamedi, International Journal of Hydrogen Energy 34 (2009) 2015–2025.
[16] Y. Yi, A.D. Rao, J. Brouwer, G.S. Samuelsen, Journal of Power Sources 132 (2004) 77–85.
[17] D. Tucker, R. Lawson, J. Vanosdol, J. Kislear, A. Akinbobuyi, Examination of Ambient Pressure Effects on Hybrid Solid Oxide Fuel Cell Turbine System Operation using Hardware Simulation, Turbo Expo 2006, 2006, Asme Paper No. Gt2006-91291.
[18] R.A. Robert, J. Brouwer, G.S. Samuelson, Fuel Cell/Gas Turbine Hybrid System Control for Daily Load Profile and Ambient Condition Variation, Turbo Expo 2006, 2006, Asme Paper No. Gt2006-90741.
[19] P. Costamagna, L. Magistri, A.F. Massardo, Journal of Power Sources 96 (2001) 352–368.
[20] M. Shelton, I. Celik, E. Liese, D. Tucker, L. Lawson, Proceedings of Turbo Expo 2005 Power for Land Sea and Air, Reno-Tahoe, NV, USA, June 6–9, 2005, Asme Paper No. Gt2005-68467.
[21] F. Mueller, R. Gaynor, A.E. Auld, J. Brouwer, F. Jabbari, G.S. Samuelsen, Journal of Power Sources 176 (1) (2008) 229–239.
[22] R.W. Fox, A.T. Mcdonald, Introduction to Fluid Mechanics, John Wiley & Sons, Inc., 1999, pp. 359–361.
[23] F.P. Incropera, D.P. Dewitt, Introduction to Heat Transfer, 5th edn, John Wiley & Sons, Inc., 2006, pp. 458–460.
[24] S.C. Chapra, Applied Numerical Methods with Matlab, 2nd edn, McGraw Hill, 2008, 460 pp.
[25] P. Costamagna, K. Honegger, Journal of the Electrochemical Society 145 (11) (1998) 3995–4007.
[26] S. Ahmed, C. Mcpheeters, R. Kumar, Journal of the Electrochemical Society 138 (9) (1991) 2712–2718.
[27] L. Petruzzi, S. Cocchi, F. Fineschi, Journal of Power Sources 118 (1–2) (2003) 96–107.
[28] M. Iwata, T. Hikosaka, M. Morita, T. Iwanari, K. Ito, K. Onda, Y. Esaki, Y. Sakaki, S. Nagata, Solid State Ionics 132 (3–4) (2000) 297–308.
[29] J.R. Ferguson, J.M. Fiard, R. Herbin, Journal of Power Sources 58 (2) (1996) 109–122.